A Finite–Element Model for the Analysis of Wrinkled Membrane Structures

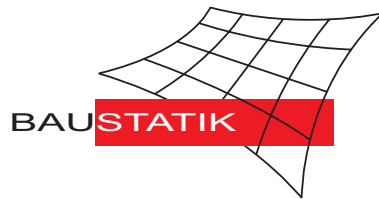**R. Ziegler, W. Wagner, K.-U. Bletzinger**

BAUSTATIK

Universität Karlsruhe (TH)
Institut für Baustatik

A Finite–Element Model for the
Analysis of Wrinkled Membrane Structures

R. Ziegler, W. Wagner, K.-U. Bletzinger

Mitteilung 1(2002)

A FINITE-ELEMENT MODEL FOR THE
ANALYSIS OF WRINKLED MEMBRANE STRUCTURES

R. Ziegler, W. Wagner, K.-U. Bletzinger

René Ziegler
Waagner Biró Stahl-Glas-Technik AG, Wien, Austria
e-mail: rziegler@wbag.co.at

Werner Wagner
Institut für Baustatik, Universität Karlsruhe (TH), Germany
e-mail: ww@bs.uni-karlsruhe.de

Kai-Uwe Bletzinger
Lehrstuhl für Statik, Technische Universität München, Germany
e-mail: kub@bv.tum.de

Abstract The problem of wrinkling in membrane structures has been a field of research since the publication of the tension field theory for plane structures. Significant progress in wrinkling analysis of arbitrarily shaped membranes has been made with the development of numerical methods. In the paper we present the enhancements of a standard finite element membrane formulation which allow to depict the wrinkles within the plane of the structure. A mathematical-numerical method is derived, which describes a valid stress state by minimizing the differences in the stress density function while observing the wrinkling conditions. A consistent linearization of the proposed algorithms ensures quadratic convergence behaviour.

1   Introduction

The form finding of membrane structures is the quest of the optimal shape. The construction material is very thin which leads to a negligible bending stiffness. All loading is supported only by tensile in-plane stresses. Compressive stresses are avoided by out-of-plane displacements known as folds and wrinkles, resulting in a nonlinear relationship between external loads $\mathbf{F}$ and the displacements $\mathbf{u}$ as shown in Fig. 1.

A load carrying structure is achieved by putting together the initially plane membrane strips to a three dimensional surface and applying an initial stress. The purely tensile stresses within the membrane enable the optimal exploitation of the highly developed coated membranes. Thus truly lightweight structures, suitable for spanning large areas, are possible.

Methods for the analysis of membrane structures undergoing large displacements are necessary for the efficient design of textile structures in architecture. The recognition and solution of the wrinkling problem of membrane structures has been a field of research since Wagner's [1] publication of the tension field theory for plane structures. Extensions of that formulation were proposed e.g. by Stein and Hedgepeth [2] for partly wrinkled and by Yokoo et
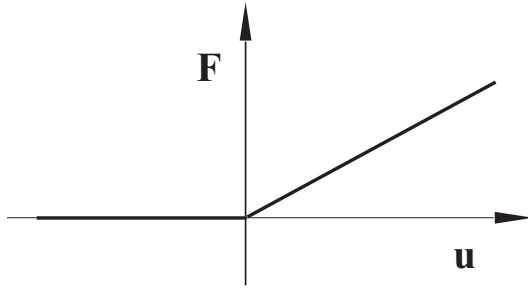
Figure 1: Unilateral load displacement relation.

al. [3] for rotational surfaces. Significant progress in wrinkling analysis of arbitrarily shaped membranes has been made with the development of numerical methods. Here, one can distinguish between two different approaches to model wrinkles in the numerical scheme. One approach is the description of the kinematics of the wrinkles within the membrane surface, as proposed e.g. by Moriya and Uemura [4], Haug and Powell [5], Pipkin [6] and Roddeman [7]. The other approach is to follow the wrinkled topology in a discrete manner, see e.g. Bauer [8], Teng et al. [9] and Cirak et al. [10, 11].

The analysis of textile structures has to include geometrically nonlinear effects due to the fact that membranes adjust to actual load conditions with large displacements. Arbitrary geometries may be modelled by the finite element method making it to an indispensable tool for the statical analysis of membrane structures. A finite element mesh with geometrical nonlinear membrane elements allows to simulate larger folds, but the smaller ones are not sufficiently captured due to the inherent length scale. In the present paper our goal is to enhance a standard finite element membrane formulation. We will extend the kinematics in order to be able to depict the wrinkles within the plane of the structure. A mathematical-numerical method is than presented for the accurate calculation of deflections, stresses and associated wrinkled states. A valid stress state is calculated by minimizing the differences in the stress density function while observing the wrinkling conditions. A consistent linearization of the proposed algorithms ensures quadratic convergence behaviour.

2 Basic relations

A geometrical nonlinear membrane has a priori the ability to approximate the geometric–morphological properties of large folds. The much smaller wrinkles that are often observed on membrane structures cannot be modelled due to the inherent length scale of the element. Using a phenomenological approach, a conventional membrane formulation will be enhanced for the analysis of membrane structures with wrinkled regions.

The wrinkling state of the membrane is determined by evaluating a criteria based on the principle stresses in the setting $\sigma_1 > \sigma_2$ as show in Tab. 1.

We will distinguish between stresses within a taut domain and those outside of this domain. Reverting to the wrinkling criteria in Tab. 1, the wrinkle free region will be identified by evaluating the principle stress state

$$f_1 := -\sigma_1 \leq 0 \qquad \text{and} \qquad f_2 := -\sigma_2 \leq 0 \quad . \tag{1}$$

2

stress state	folds	membrane
$\sigma_2 > 0$	none	taut
$\sigma_1 > 0$ and $\sigma_2 < 0$	uniaxial	folded
$\sigma_1 \leq 0$	biaxial	slack

Table 1: wrinkling criteria in principle stresses

The valid stress states $\boldsymbol{\sigma}$ of the taut domain $\mathbf{E}_{\boldsymbol{\sigma}}$ are bounded by the principle stresses in the sense

$$\mathbf{E}_{\boldsymbol{\sigma}} := \{\boldsymbol{\sigma} \subset \mathbf{S} \mid f_\alpha(\boldsymbol{\sigma}) \leq 0 \quad \text{for all} \quad \alpha \in \{1,2\}\} \tag{2}$$

with f_1 and f_2 as continuous, independent functions.

A load case causing the membrane structure to wrinkle will be possible. In order to describe the kinematics of the wrinkled membrane the strain tensor $\boldsymbol{\varepsilon}$ is decomposed in analogy to an elasto–plastic scheme into a taut part $\boldsymbol{\varepsilon}^e$ and a wrinkled part $\boldsymbol{\varepsilon}^w$

$$\boldsymbol{\varepsilon} = \boldsymbol{\varepsilon}^e + \boldsymbol{\varepsilon}^w \quad . \tag{3}$$

The stresses will be derived from the strain-energy function

$$\boldsymbol{\sigma} = \frac{\partial}{\partial \boldsymbol{\varepsilon}} W(\boldsymbol{\varepsilon} - \boldsymbol{\varepsilon}^w) . \tag{4}$$

Based on the elastic moduli $\mathbb{C}$ it holds

$$\boldsymbol{\sigma} = \mathbb{C} : (\boldsymbol{\varepsilon} - \boldsymbol{\varepsilon}^w) . \tag{5}$$

Since the wrinkle strains are initially unknown, a trial stress state will be calculated with

$$\boldsymbol{\sigma}^{trial} = \mathbb{C} : \boldsymbol{\varepsilon} . \tag{6}$$

If $f_\alpha(\boldsymbol{\sigma}^{trial}) \leq 0$ for all $\alpha \in \{1,2\}$ a valid stress state has been found and

$$\boldsymbol{\sigma} = \boldsymbol{\sigma}^{trial} . \tag{7}$$

The membrane is taut. If one of the two conditions in Eq. (1) is violated, the calculated stress state will not be located within the valid region and the membrane will be wrinkled or slack. A new stress state $\boldsymbol{\sigma}$ which fulfill these conditions has to be found, see Fig. 2. Simo and Hughes [12] propose a solution for a similar problem minimizing the strain energy function

$$W(\boldsymbol{\sigma}) = \frac{1}{2} \quad \boldsymbol{\sigma} : \mathbb{C}^{-1} : \boldsymbol{\sigma} . \tag{8}$$

For a valid response of the membrane, the obtained stress state has to be located within the taut domain. Starting with an initial trial state $\boldsymbol{\sigma}^{trial}$ using the closest point projection [13] in the energy norm a valid stress response $\boldsymbol{\sigma}$ is obtained by

$$\chi(\boldsymbol{\sigma}) := \frac{1}{2}(\boldsymbol{\sigma}^{trial} - \boldsymbol{\sigma}) : \mathbb{C}^{-1} : (\boldsymbol{\sigma}^{trial} - \boldsymbol{\sigma}) \qquad \rightarrow \min . \tag{9}$$

Furthermore it will be described as the solution of a convex mathematical programming problem and is reduced to a standard problem of finding the closest distance in the energy

norm of a trial state to the taut domain. With χ as the objective function and considering the constraint conditions (1) the Lagrangian $\mathcal{L}$ is denoted as

$$\mathcal{L}(\boldsymbol{\sigma}, \lambda) = \chi(\boldsymbol{\sigma}) + \lambda^\alpha f_\alpha \qquad \rightarrow \text{stat.} \tag{10}$$

The solution is derived from the variation of $\mathcal{L}(\boldsymbol{\sigma}, \lambda)$ yielding the derivatives

$$\partial_{\boldsymbol{\sigma}} \mathcal{L} = -\mathbb{C}^{-1} : (\boldsymbol{\sigma}^{trial} - \boldsymbol{\sigma}) + \lambda^\alpha \partial_{\boldsymbol{\sigma}} f_\alpha = \boldsymbol{0} \tag{11}$$

and

$$\partial_{\lambda^\alpha} \mathcal{L} = f_\alpha \leq 0 \tag{12}$$

with the Kuhn–Tucker conditions

$$\lambda^\alpha \geq 0 \quad \text{and} \quad \lambda^\alpha f_\alpha = 0 \quad . \tag{13}$$

The Lagrange parameter λ^α will be derived by Eqns. (11–13) with the active set of conditions. The optimality conditions (11, 12) will be linearized for the calculation of the active Lagrange parameters λ^α using a Newton–Raphson scheme. Solving the Lagrangian with the Newton–Raphson algorithm in a straightforward manner yields an admissible stress state within the elastic domain. Handling the multisurface problem, active constraint surfaces have to be taken into account, which are not known in advance. The procedure indicated above is applied whenever one of the constraints is active and furthermore it will be observed if they remain active throughout the process.

3 Solution algorithm and implementation

When using the proposed model to solve the discrete problem, the following three aspects have to be considered:

(i) The Lagrange parameters λ^α and the actual stress state $\boldsymbol{\sigma}$ have to be calculated on the local (Gauss point) level.

(ii) Within the geometrically nonlinear formulation of the structure the term $\frac{d\boldsymbol{\sigma}}{d\boldsymbol{\varepsilon}}$ have to be calculated.

(iii) This linearization requires the derivatives of the constraint equations with respect to the stresses. Thus, constraints f_α should be provided as functions of the stress tensor $\boldsymbol{\sigma}$.

3.1 Local Newton–Raphson iteration

The following box contains the main steps in the local iteration to find admissible stresses.

1. Calculate current state
$$\boldsymbol{\sigma}^{trial} \;=\; \mathbb{C} : \boldsymbol{\varepsilon}$$
$$f_\alpha^{trial} \;:=\; f_\alpha(\boldsymbol{\sigma}^{trial}) \quad \text{for all} \quad \alpha \in \{1,2\}$$

2. Check constraints

   IF $\;f_\alpha^{trial} \leq 0$ for all $\alpha \in \{1,2\}$ THEN
   $$\boldsymbol{\sigma} = \boldsymbol{\sigma}^{trial} \quad \text{EXIT}$$
   ELSE
   $$\mathbf{J}_{act}^{(0)} \;:=\; \{\alpha \in \{1,2\} | f_\alpha^{trial} > 0\}$$
   $$\boldsymbol{\sigma}^{(0)} \;=\; 0$$
   $$\lambda^{\beta^{(0)}} \;=\; 0$$
   ENDIF

3. Evaluate residual
$$\mathbf{R}^{(k)} \;=\; -\mathbb{C}^{-1} : (\boldsymbol{\sigma}^{trial} - \boldsymbol{\sigma}^{(k)}) + \lambda^{\beta^{(k)}} \partial_\sigma f_\beta^{(k)} \quad \text{for all} \quad \beta \in \mathbf{J}_{act}^{(k)}$$

4. Check convergence
$$\text{IF} \quad f_\alpha^{trial} < \text{TOL}_1 \text{ for all } \alpha \in \mathbf{J}_{act} \text{ and } ||\mathbf{R}^{(k)}|| < \text{TOL}_2 \quad \text{EXIT}$$

5. Compute tangent moduli
$$[G_{\alpha\beta}]^{(k)} \;:=\; \left[\partial_\sigma f_\alpha^{(k)}\right] : \bar{\mathbb{C}} : \left[\partial_\sigma f_\beta^{(k)}\right]$$
$$\left[G^{\alpha\beta}\right]^{(k)} \;:=\; [G_{\alpha\beta}]^{(k)^{-1}}$$
$$\bar{\mathbb{C}}^{-1} \;:=\; \mathbb{C}^{-1} + \lambda^{\beta^{(k)}} \partial_{\sigma\sigma}^2 f_\beta^{(k)} \quad \text{for all} \quad \beta \in \mathbf{J}_{act}^{(k)}$$

6. Increment of Lagrangian parameters
$$\Delta\lambda^{\beta^{(k)}} \;:=\; +\left[G^{\alpha\beta}\right]^{(k)} \{f_\alpha - \partial_\sigma f_\alpha : \bar{\mathbb{C}} : \mathbf{R}\}_\beta^{(k)} \quad \text{for all} \quad \alpha \in \mathbf{J}_{act}^{(k)}$$
$$\lambda_{trial}^{\alpha^{(k+1)}} \;:=\; \lambda^{\alpha^{(k)}} + \Delta\lambda^{\alpha^{(k)}}$$

   IF $\;\lambda_{trial}^{\alpha^{(k+1)}} < 0, \quad \alpha \in \mathbf{J}_{act}^{(k)}$ THEN
   $$\mathbf{J}_{act}^{(k)} = \{\alpha \in \mathbf{J}_{act}^{(k)} \,|\, \lambda_{trial}^{\alpha^{(k+1)}} > 0\} \text{ GOTO 3}$$
   ENDIF

7. Increment of stresses
$$\Delta\boldsymbol{\sigma}^{(k)} = \bar{\mathbb{C}}^{(k)} : \left[\mathbf{R} + \Delta\lambda^\beta \partial_\sigma f_\beta\right]^{(k)} \quad \text{for all} \quad \beta \in \mathbf{J}_{act}^{(k)}$$

8. Update stresses and Lagrangian parameters
$$\boldsymbol{\sigma}^{(k+1)} \;=\; \boldsymbol{\sigma}^{(k)} + \Delta\boldsymbol{\sigma}^{(k)}$$
$$\lambda^{\alpha^{(k+1)}} \;=\; \lambda^{\alpha^{(k)}} + \Delta\lambda^{\alpha^{(k)}} \quad \alpha \in \mathbf{J}_{act}^{(k+1)}$$

   Set $k \;\leftarrow\; k + 1$ and GOTO 3

Some remarks concerning step 6 of the solution algorithm are necessary. In the case that both conditions of Eq. (1) are initially active, one has to observe if they remain active throughout the process. The reason for this behaviour can be seen considering Eqns. (11) and (13). To fulfill the Kuhn–Tucker conditions, the negative gradient of the objective function $\partial_{\boldsymbol{\sigma}} \chi$ has to be bounded by the gradients of the active set of constraints $\partial_{\boldsymbol{\sigma}} f_\alpha$. Two different possible situations are shown in Fig. 3. On the left hand side the solution of λ^α is governed by both constraints whereas on the right hand side initially two active constraints occur while only one has influence on the solution.

3.2 Tangent moduli

The weak form of equilibrium leads to a nonlinear problem which has to be solved with an iterative Newton–Raphson scheme on the entire domain of the structure. The advantage of the proposed algorithm is that it can be linearized exactly ensuring quadratic convergence behaviour, see e.g. [13]. By differentiating the elastic stress–strain relationship in Eq. (5) we obtain

$$\mathrm{d}\,\boldsymbol{\sigma} = \mathbb{C} : (\mathrm{d}\,\boldsymbol{\varepsilon} - \mathrm{d}\,\boldsymbol{\varepsilon}^w) \tag{14}$$

The linearization of Eqn. (11) denoted as $\boldsymbol{\varepsilon}^w = \lambda^\alpha \partial_{\boldsymbol{\sigma}} f_\alpha$ leads to

$$\mathrm{d}\,\boldsymbol{\varepsilon}^w = \lambda^\alpha \partial_{\sigma\sigma}^2 f_\alpha \,\mathrm{d}\,\boldsymbol{\sigma} + \partial_\sigma f_\alpha : \mathrm{d}\,\lambda^\alpha \,. \tag{15}$$

Now, Eqns. (14) and (15) can be combined to the incremental relation

$$\mathrm{d}\,\boldsymbol{\sigma} = \bar{\mathbb{C}} : [\mathrm{d}\,\boldsymbol{\varepsilon} - \partial_{\boldsymbol{\sigma}} f_\alpha : \mathrm{d}\,\lambda^\alpha] \,. \tag{16}$$

In the next step the coefficients $\mathrm{d}\,\lambda^\alpha$ will be derived from the consistency condition (13) and substituted into (16) resulting in an algorithmic tangent moduli

$$\frac{\mathrm{d}\,\boldsymbol{\sigma}}{\mathrm{d}\,\boldsymbol{\varepsilon}} = \mathbb{C}_T = \bar{\mathbb{C}} - g^{\beta\alpha} \mathbf{N}_\beta \otimes \mathbf{N}_\alpha \quad \text{for all} \quad \alpha, \beta \in \mathbf{J}_{act} \tag{17}$$
$$\text{with} \qquad \mathbf{N}_\alpha = \bar{\mathbb{C}} : \partial_{\boldsymbol{\sigma}} f_\alpha \,.$$

To calculate the tangent stiffness matrix, the algorithmic tangent moduli has to be chosen according the elements in the set of active constraints.

$$\frac{\mathrm{d}\,\boldsymbol{\sigma}}{\mathrm{d}\,\boldsymbol{\varepsilon}} = \begin{cases} \mathbb{C} & \text{if} \quad \mathbf{J}_{act} = 0 \\ \mathbb{C}_T & \text{if} \quad \mathbf{J}_{act} \neq 0 \end{cases} \tag{18}$$

3.3 Constraints and derivatives

The constraints of the proposed algorithm are defined in terms of the principle stresses, calculated from the stress tensor $\boldsymbol{\sigma}$.

For a plane–stress situation, the major principle stress σ_1 and the minor principle stress σ_2 are defined by

$$\sigma_\alpha = \left[\frac{1}{2} \boldsymbol{\pi}^T \boldsymbol{\sigma} \pm (\frac{1}{2} \boldsymbol{\sigma}^T \mathbf{P} \boldsymbol{\sigma})^{\frac{1}{2}} \right] \qquad \alpha \in \{1, 2\} \tag{19}$$
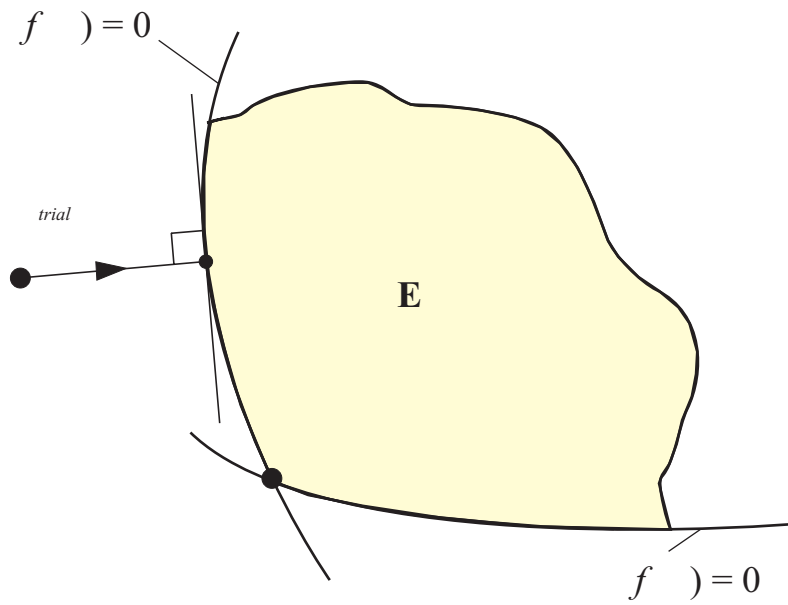
f) = 0

trial

E

f) = 0

Figure 2: Area of valid stress states and corrector step

f) = 0

f_1

f_2

f) = 0

f) = 0
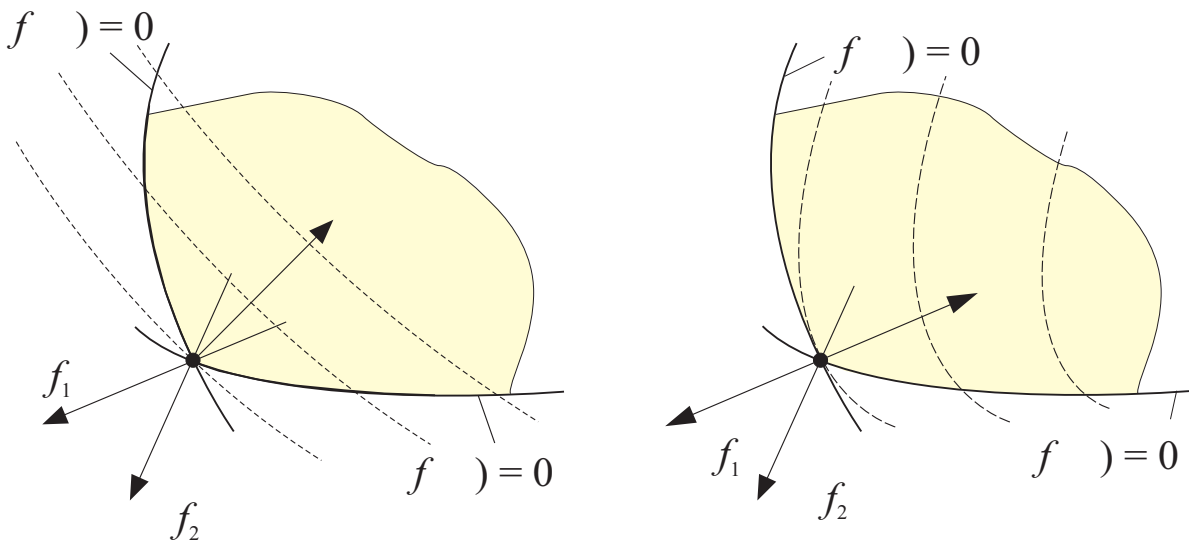
f_1

f_2

f) = 0

Figure 3: Gradients of the objective function and constraints at the intersection of the constraint conditions.
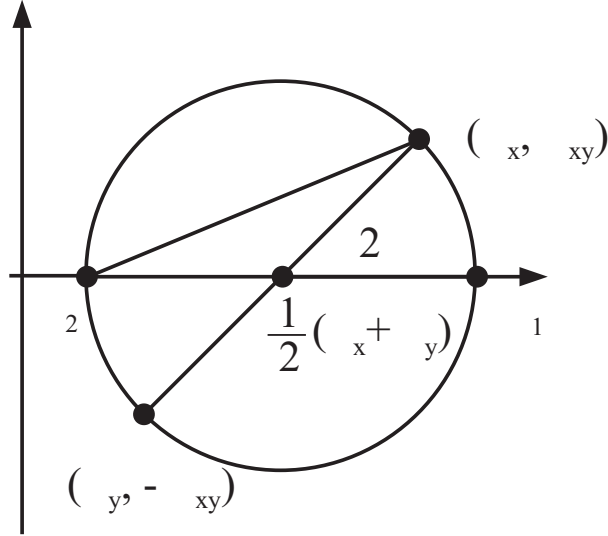
Figure 4: Mohr's circle

In Eq. (19) (+) hold for $\alpha = 1$ whereas (-) has to be chosen for $\alpha = 2$. The projection vector $\boldsymbol{\pi}$ and the projection matrix $\mathbf{P}$ are given by

$$\boldsymbol{\pi} = \begin{bmatrix} 1 & 1 & 0 \end{bmatrix}^T \qquad \mathbf{P} = \begin{bmatrix} \frac{1}{2} & -\frac{1}{2} & 0 \\ -\frac{1}{2} & \frac{1}{2} & 0 \\ 0 & 0 & 2 \end{bmatrix} \qquad (20)$$

respectively. A graphical illustration of the principal stresses can be given with Mohr's circle, see Fig. 4. Thus, the boundaries of a taut domain in Eqn. (2) can be expressed by

$$f_\alpha := -\sigma_\alpha = -\left[\frac{1}{2}\boldsymbol{\pi}^T\boldsymbol{\sigma} \pm (\frac{1}{2}\boldsymbol{\sigma}^T\mathbf{P}\boldsymbol{\sigma})^{\frac{1}{2}} \right] \qquad \alpha \in \{1,2\}. \qquad (21)$$

The necessary first and second derivatives of the constraint equations are calculated straightforward

$$\partial_{\boldsymbol{\sigma}} f_\alpha = -\frac{1}{2}\boldsymbol{\pi}^T \mp \frac{\mathbf{P}\boldsymbol{\sigma}}{2\left(\frac{1}{2}\boldsymbol{\sigma}^T\mathbf{P}\boldsymbol{\sigma}\right)^{\frac{1}{2}}} \qquad \alpha \in \{1,2\}, \qquad (22)$$

and

$$\partial^2_{\boldsymbol{\sigma}\boldsymbol{\sigma}} f_\alpha = \mp \frac{\mathbf{P}}{2\Psi} \pm \frac{\mathbf{P}\boldsymbol{\sigma}\,\boldsymbol{\sigma}^T\mathbf{P}}{4\Psi} \qquad \alpha \in \{1,2\} \qquad (23)$$

with $\Psi = (\frac{1}{2}\boldsymbol{\sigma}^T\mathbf{P}\boldsymbol{\sigma})^{\frac{1}{2}}$.

4   Numerical examples

In this section we present some numerical simulations to illustrate the performance of the proposed algorithms. These are a Hp-Membrane under dead load, an airbag under internal pressure and a more complicated pneumatic structure under internal pressure. The derived formulations are implemented in a 4–node isoparametric bilinear element which is part of an enhanced version of the general purpose non–linear finite element program FEAP, see Zienkiewicz and Taylor [16].

4.1 HP Membrane

The following system is chosen in accordance to a problem initially analyzed by Bauer [8]. The material properties and dimensions of the undeformed system are shown in Fig. 5. The membrane is simply supported along all edges.

$$
\begin{array}{rl}
\text{length} & a = 12\sqrt{2}\,m \\
\text{height} & b = 2.88\,m \\
\text{thickness} & t = 0.03\,cm \\
\text{elastic modulus} & E = 21 \cdot 10^3\,kN/cm^2 \\
\text{poisson's ratio} & \nu = 1/3
\end{array}
$$
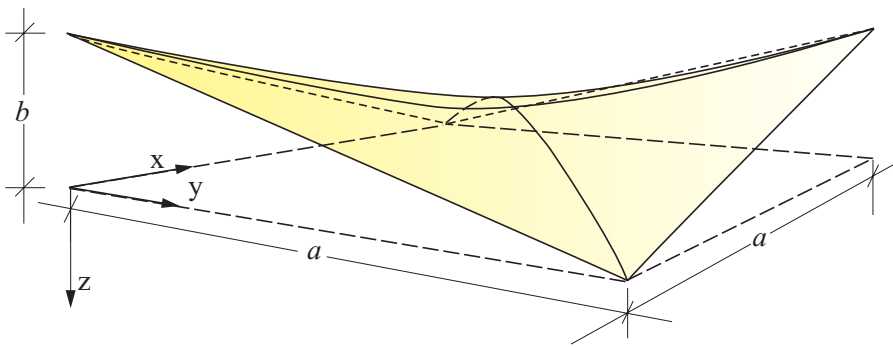
Location:
M in center
A, B in quarter points
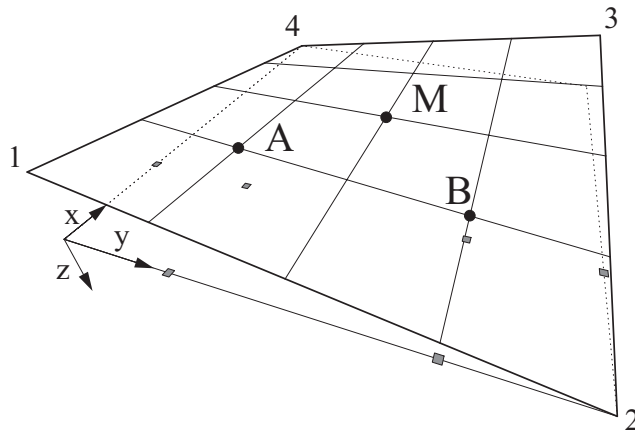
Figure 5: hp–membrane: system and observed points

A distributed load in z–direction is applied and will be successively increased to a maximum value of $10\,kN/m^2$ within a Newton procedure. Throughout the deformation process the displacements of points A, B and M in load direction will be observed. To illustrate the nonlinear behaviour of the load–bearing the principle stresses $\sigma_{1,2}$ and the principle wrinkle strains $\varepsilon^w_{1,2}$ indicating the wrinkled areas are displayed in Figures 8-10 . The computation is performed on a converged mesh with 256 elements. The specific load–bearing characteristic of membranes is observed immediately after applying load in Fig. 7. In order to achieve a state of equilibrium with tensile stresses, the membrane has to assume a deflection state comparable to the catenary for the two dimensional rope.
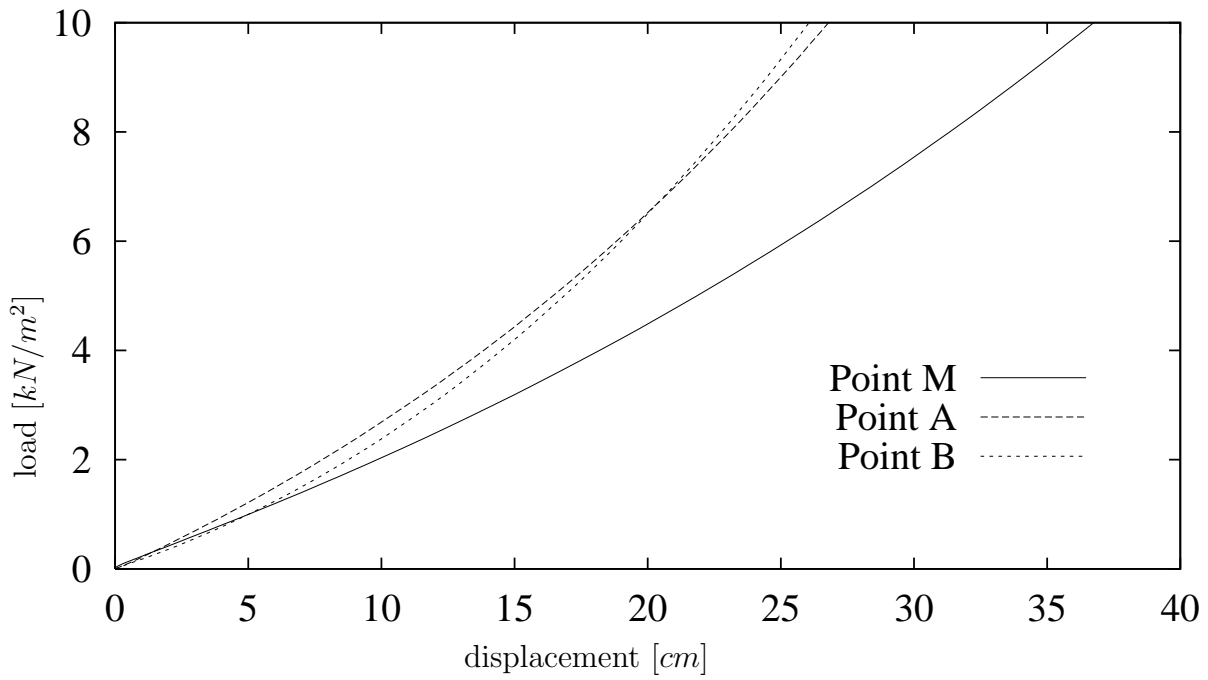
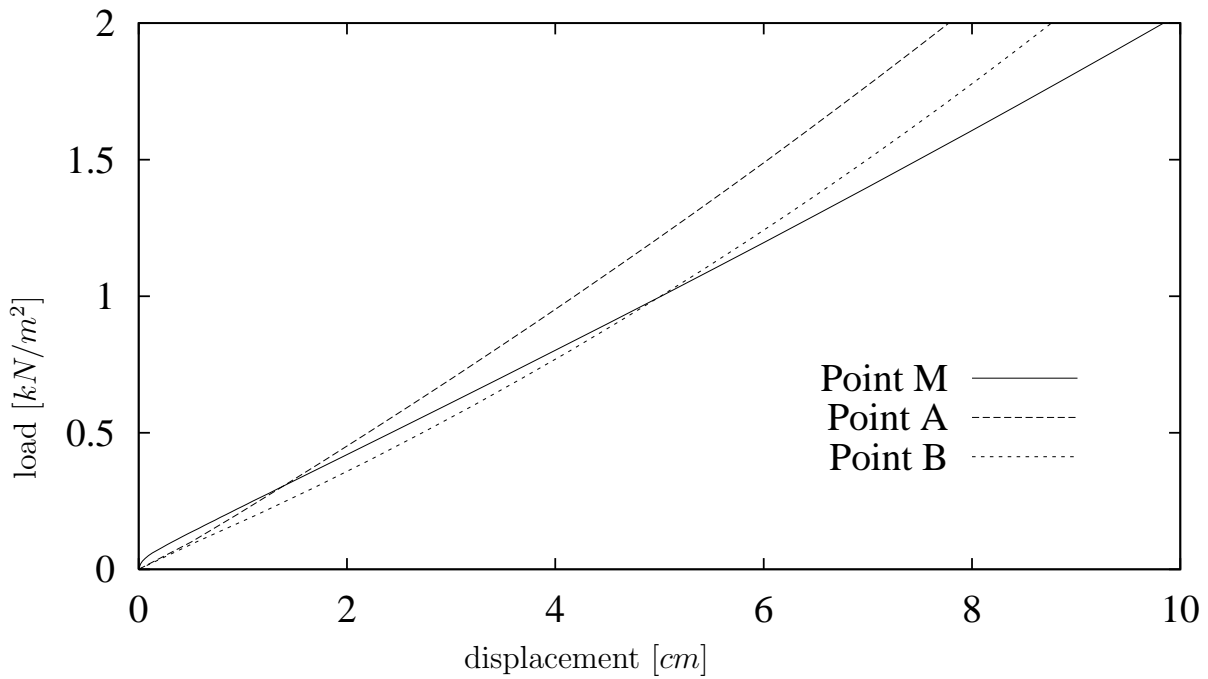Figure 6: Vertical displacements of points A, B, M.

Figure 7: Vertical displacements of points A, B, M in the load range $(0$–$2\ kN/m^2)$.
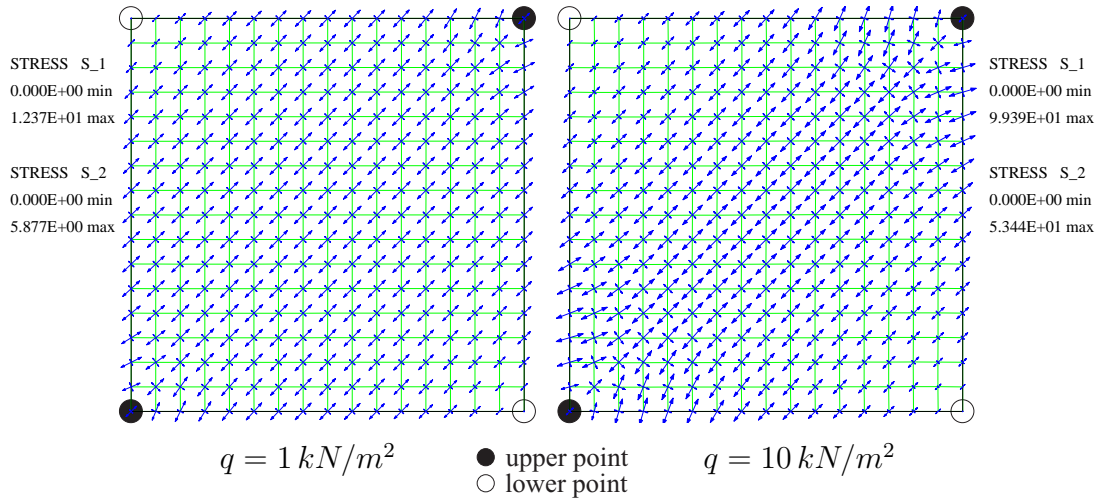
STRESS S_1

0.000E+00 min

1.237E+01 max

STRESS S_2

0.000E+00 min

5.877E+00 max

STRESS S_1

0.000E+00 min

9.939E+01 max

STRESS S_2

0.000E+00 min

5.344E+01 max

$q = 1\,kN/m^2$ ● upper point $q = 10\,kN/m^2$
○ lower point

Figure 8: Principle stresses for $q = 1\,kN/m^2$ and $q = 10\,kN/m^2$.

WRINKLE 1

-3.468E-06 min

3.726E-07 max

WRINKLE 2

-1.546E-05 min

0.000E+00 max

WRINKLE 1

-2.630E-05 min

4.136E-06 max

WRINKLE 2

-9.195E-05 min

0.000E+00 max

$q = 0.01\,kN/m^2$ ● upper point $q = 0.1\,kN/m^2$
○ lower point
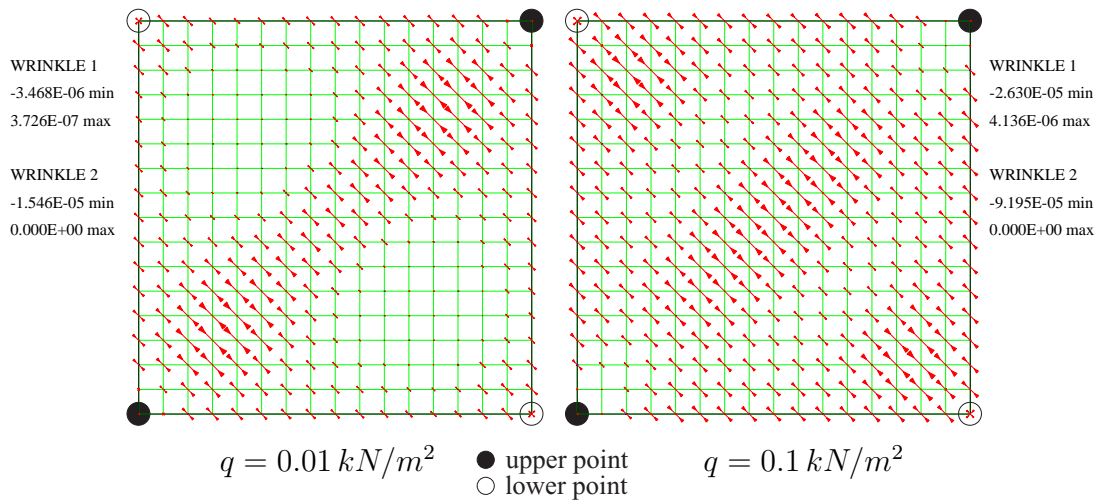
Figure 9: Principle wrinkle strains $\varepsilon_{1,2}^{w}$ for $q = 0.01\,kN/m^2$ and $q = 0.1\,kN/m^2$.

11

WRINKLE 1
-1.399E-04 min
2.710E-05 max

WRINKLE 2
-8.309E-04 min
0.000E+00 max

WRINKLE 1
-6.797E-04 min
1.455E-04 max

WRINKLE 2
-5.255E-03 min
0.000E+00 max

$q = 1\,kN/m^2$ ● upper point $q = 10\,kN/m^2$
○ lower point
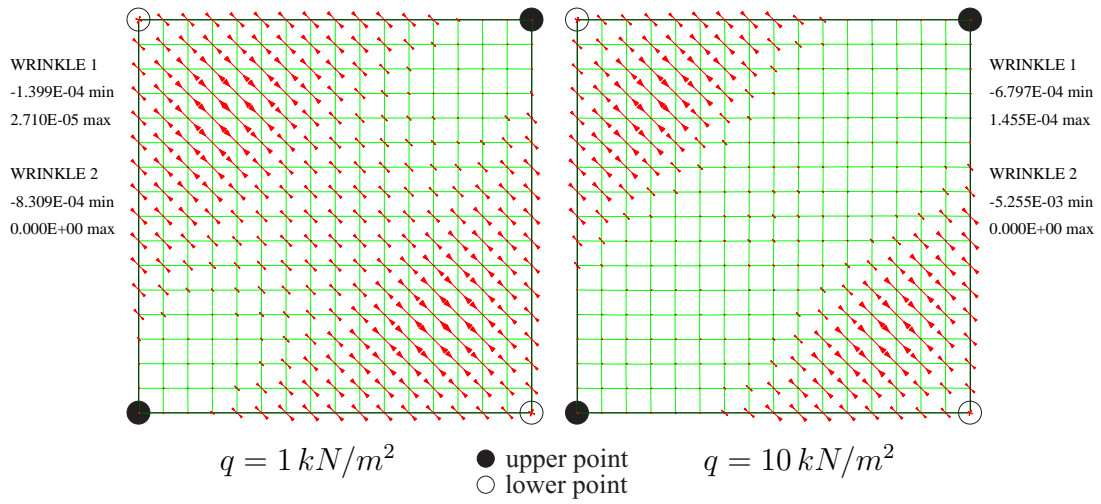
Figure 10: Principle wrinkle strains $\varepsilon_{1,2}^w$ for $q = 1\,kN/m^2$ and $q = 10\,kN/m^2$.

4.2 Inflated airbag

As a further application of the procedure outlined above, an inflated airbag, shown in Fig. 11, is analyzed. The airbag consists of an isotropic elastic material with very low flexural stiffness which is therefore assumed to be zero. The airbag consists of two square plane membranes which are welded together along the edges. By applying appropriate boundary conditions in the horizontal midplane, it is only necessary to model the upper part of the membrane. The same problem was analyzed by Bauer [8] and Contri and Schrefler [14]. The calculations were performed on successively refined meshes. To simulate the internal pressure p_i a non–conservative loading scheme was applied [15].

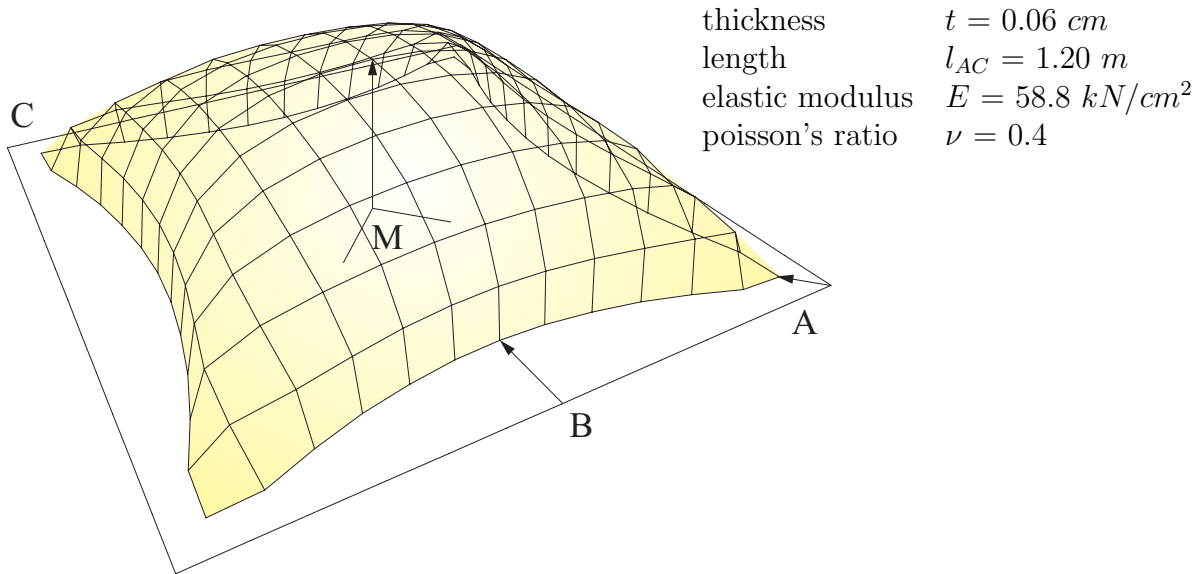| thickness | $t = 0.06\ cm$ |
length	$l_{AC} = 1.20\ m$
elastic modulus	$E = 58.8\ kN/cm^2$
poisson's ratio	$\nu = 0.4$

Figure 11: Inflated airbag: system and material properties

The process of inflating the flat membrane immediately raises the structure to a pillow position due to the fact that equilibrium with zero flexural stiffness will not be achieved in intermediate positions. The calculations are carried out in a straightforward manner. The results will be compared to those performed by Bauer [8] and Contri and Schrefler [14].

	Bauer [8]	C&S [14]	proposed algorithm				
num. elements	256	100	16	64	144	256	400
$f_M\ [cm]$	20.5	21.7	21.2	21.5	21.6	21.6	21.6
$f_A\ [cm]$	4.7	6.3	10.6	9.7	8.2	7.4	6.9
$f_B\ [cm]$	13.0	11.0	11.8	12.0	12.1	12.2	12.3
$\sigma_M\ [kN/cm^2]$	0.35	0.35	0.27	0.36	0.36	0.37	0.37

Table 2: Displacements A, B, C and stress σ_M at $p_i = 5\ kN/m^2$.

The results shown in Table 2 indicate that even with a very coarse discretization, a qualitatively adequate description of the deflection can be made. The distinction between elastic and wrinkle strains enables the visualization of the wrinkled areas in a post processing procedure.
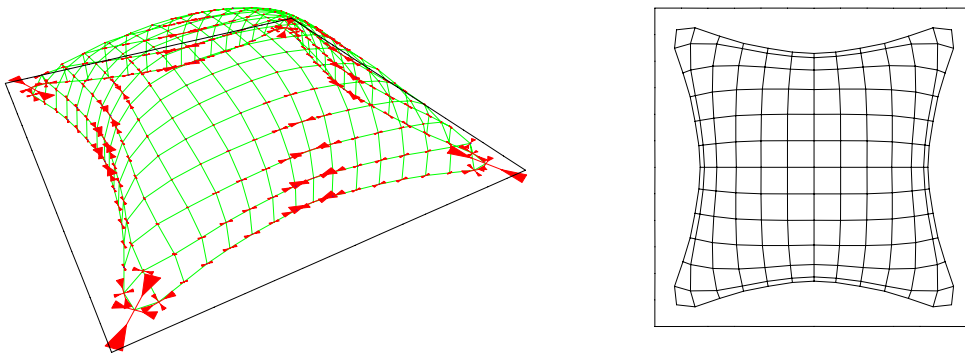
Figure 12: Principle wrinkle strains and top view of the deformed mesh at $p_i = 5\,kN/m^2$

Fig. 12 clearly shows the regions where wrinkling occurs. It is important to observe, that the results are not mesh dependent and there are no compressive stresses. Convergence behaviour can be studied on displacement–pressure curves in Figures 13–15.
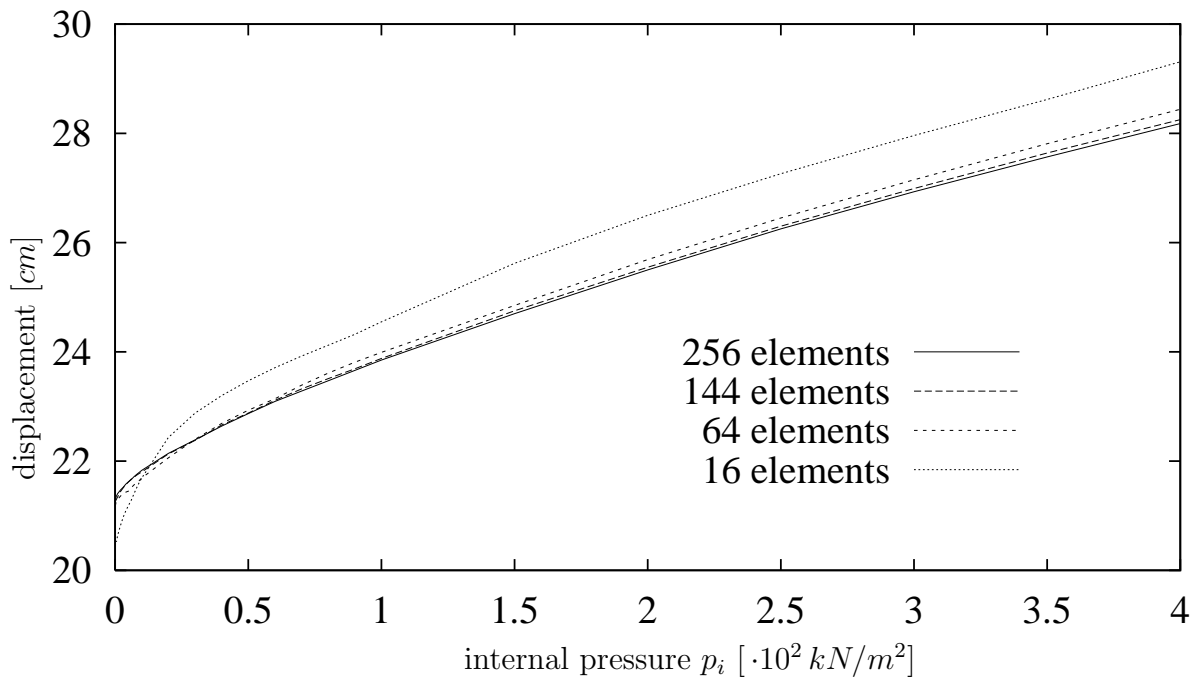

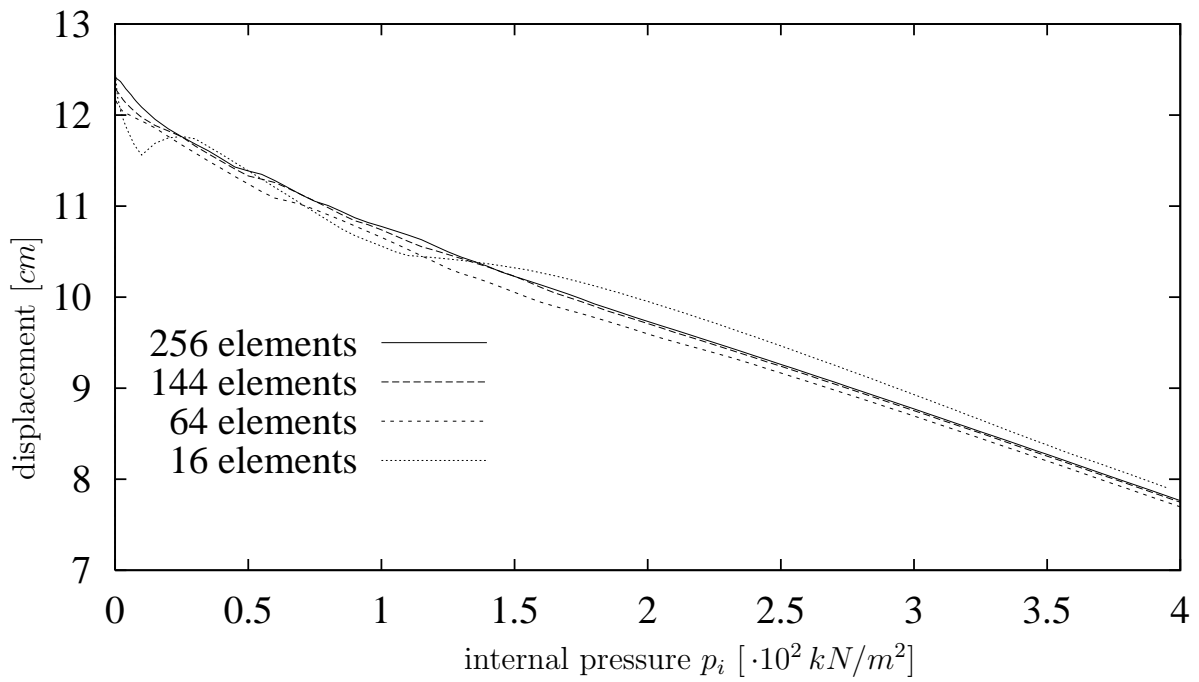Figure 13: Vertical displacement f_M of point M
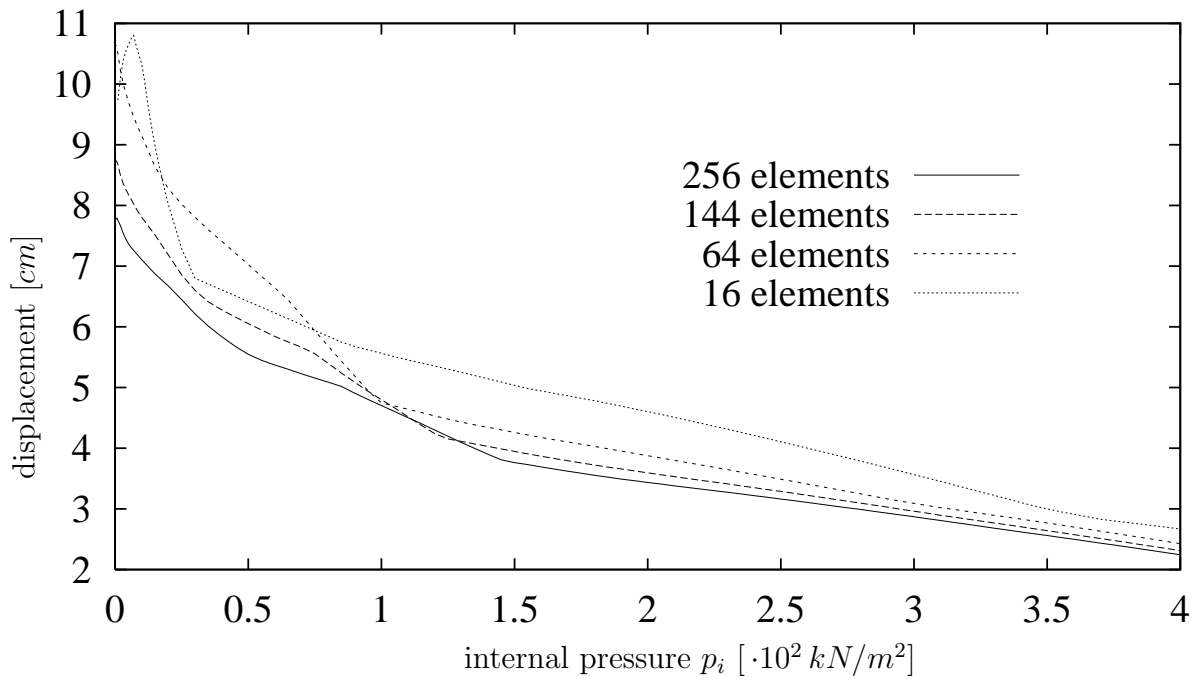
Figure 14: Horizontal displacement f_B of point B

Figure 15: Horizontal displacement f_A of point A

4.3 Pneumatic structure

The third example is an initially flat cross shaped membrane bag, which is subjected to internal pressure. For the calculations the isotropic material behaviour of the previous structure has been assumed. Again by applying the appropriate boundary conditions in mid–plane only the upper part of the membrane has to be modelled.

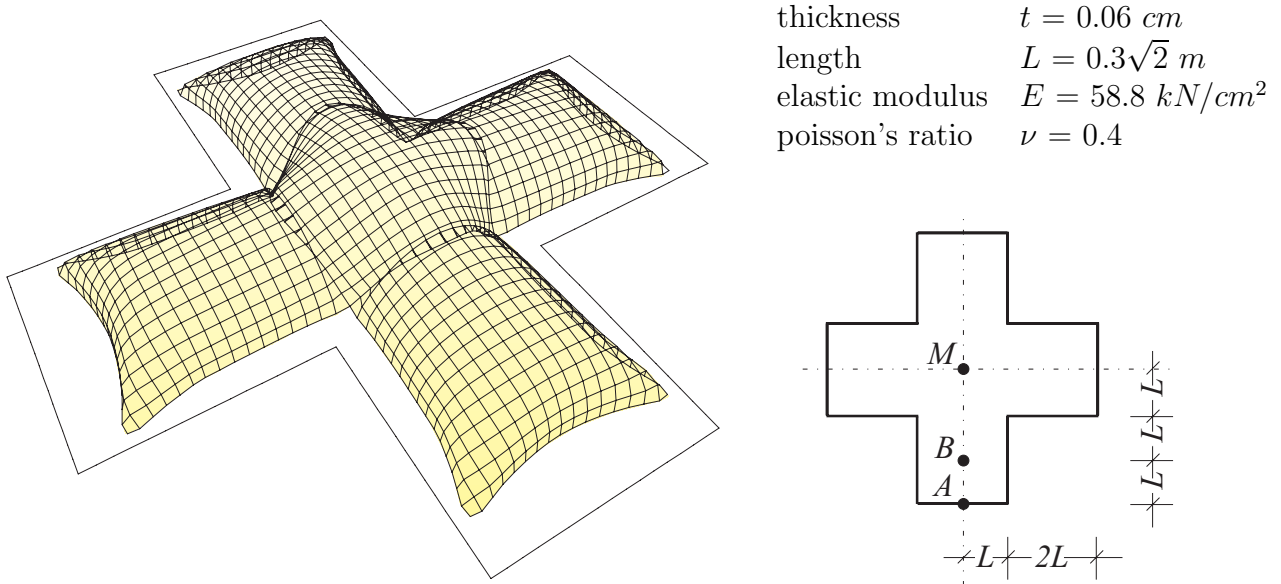| thickness | $t = 0.06\ cm$ |
length	$L = 0.3\sqrt{2}\ m$
elastic modulus	$E = 58.8\ kN/cm^2$
poisson's ratio	$\nu = 0.4$

Figure 16: Pneumatic structure: system and material properties

The behavior of the structure is characterized by the well–defined wrinkling in the intersection areas in the early stage of inflation. As the internal pressure p_i increases the wrinkling disappears, only the wrinkle strains previously discussed in the corners remain. Again the convergence behaviour can be studied on displacement–pressure curves in Figures 18–20.
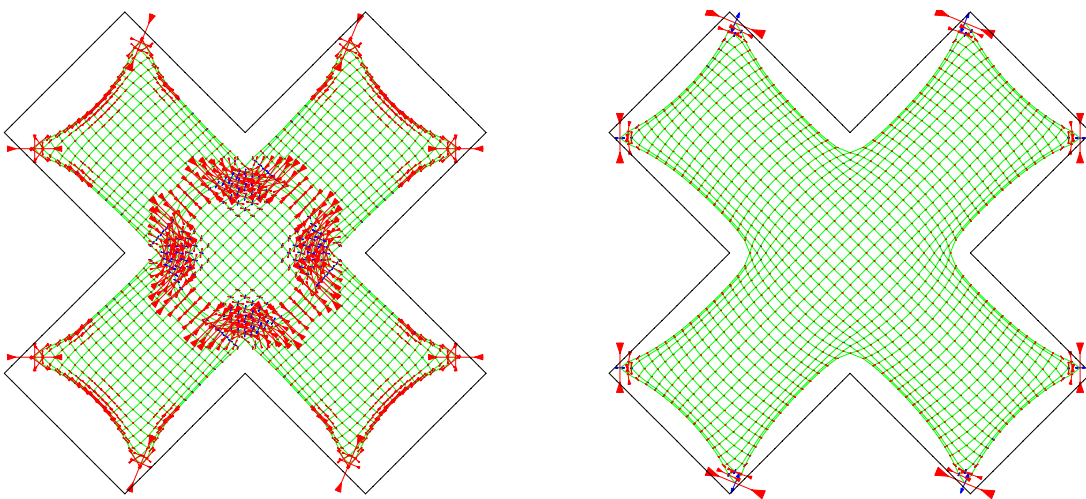

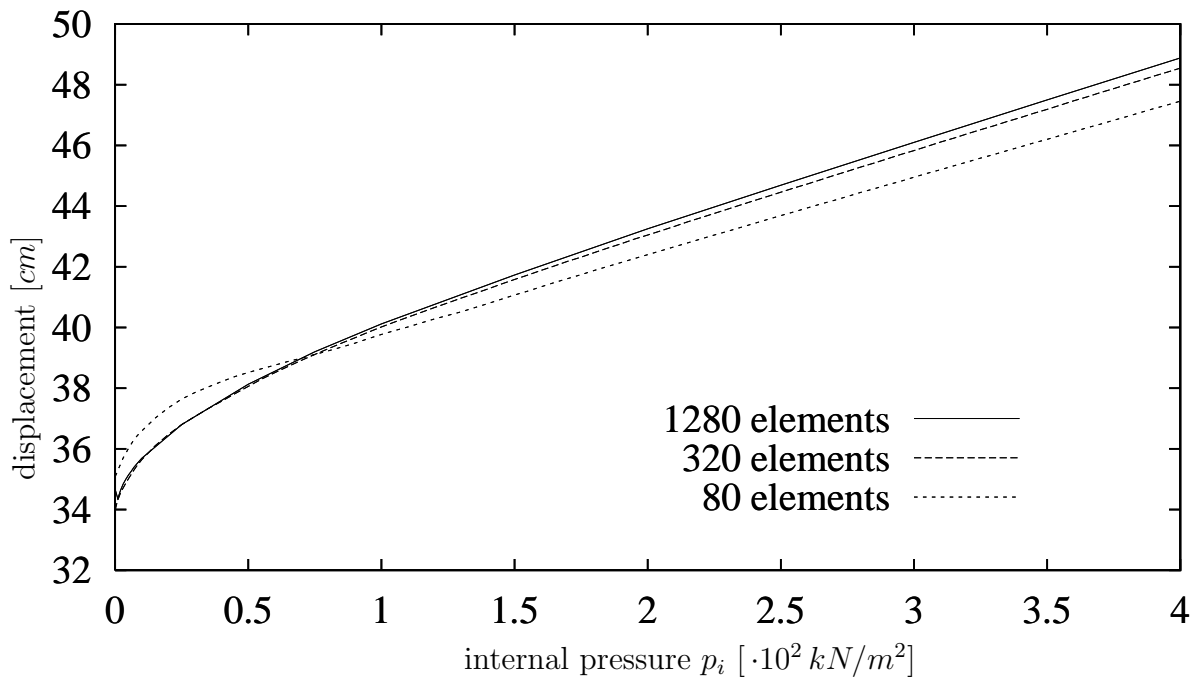Figure 17: Wrinkle strains at $p_i = 5\ kN/m^2$ and $p_i = 150\ kN/m^2$
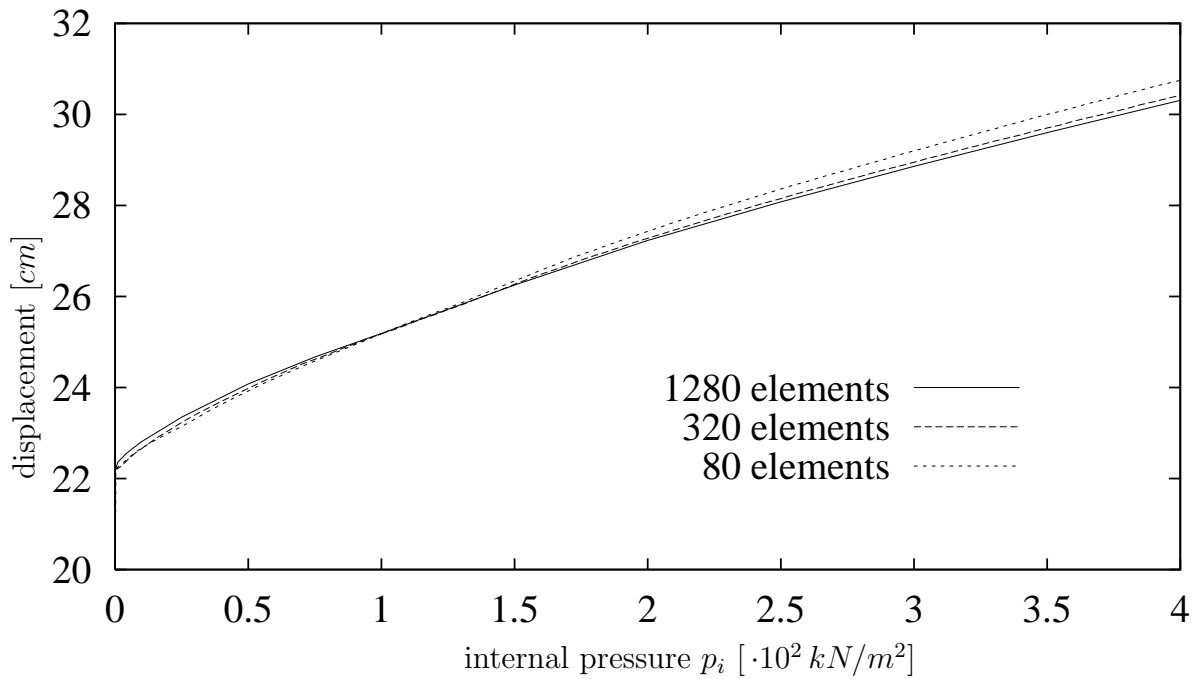
Figure 18: Vertical displacement f_M of point M

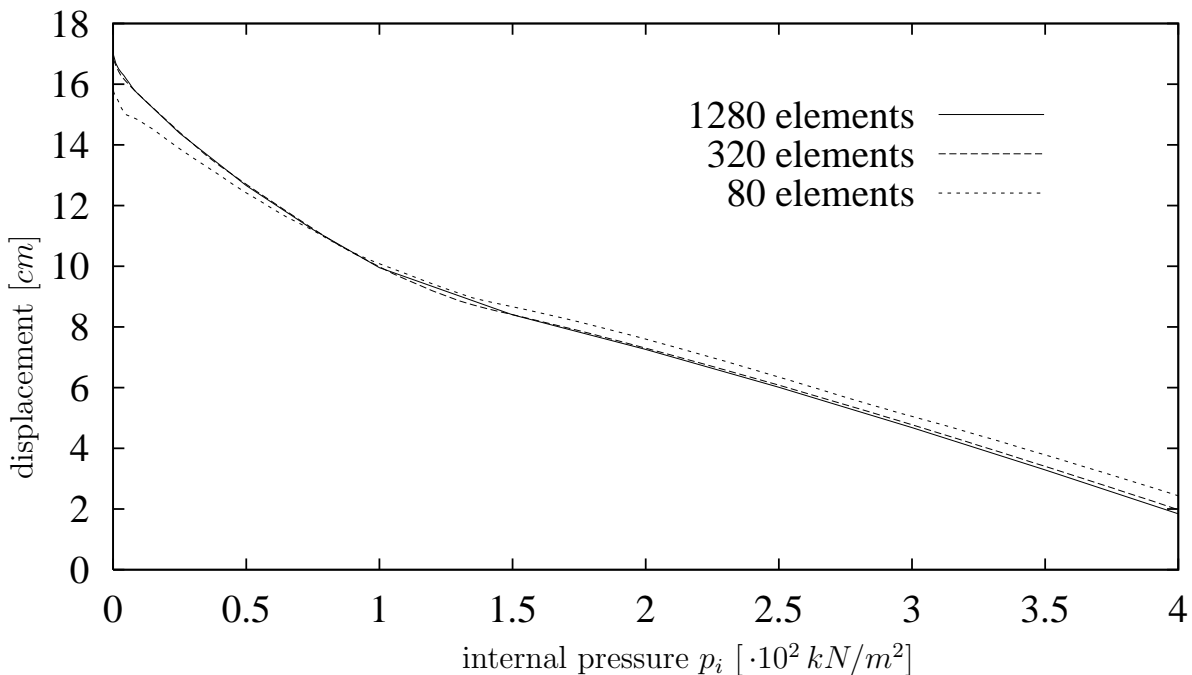Figure 19: Vertical displacement f_B of point B

17

Figure 20: Horizontal displacement f_A of point A

5 Conclusions

The curvature and the pre-tensioning of the membrane define the load carrying capacity of membrane structures. Ideally one obtains only tensile stresses in the membrane during the loading. However for some load cases wrinkles may occur. In this paper a mechanical model and its numerical implementation for the description of wrinkles within the structural plane of the membrane is presented. The strains are decomposed into an elastic and an inelastic wrinkling part. The domain of admissible stresses is bounded by two independent constraints derived from a wrinkling criteria. The formulation is similar to algorithms of plasticity and contains a local Newton iteration to satisfy the wrinkling conditions. The algorithmic tangent modulus ensures quadratic convergence of the global equilibrium Newton iteration. The numerical examples show that the model is applicable for scientific as well as engineering purposes.

References

[1] H. Wagner. Flat sheet metal girders with a very thin metal web. *Zeitschrift für Flugtechnik und Motorluftschiffahrt*, 20:200–207, 1929.

[2] M. Stein and J.M. Hedgepeth. Analysis of partly wrinkled membranes. In *NASA Technical Note D - 813*, Washington, 1961.

[3] Y. Yokoo, H. Matsunage and Y. Yokoyama. On the behavior of wrinkled regions of pneumatic membranes in the form of a surface of revolution under symmetrical loading.

In *IASS Pacific Symposium - Part II On Tension Structures and Space Frames*, Tokyo and Kyoto, 1971.

[4] K. Moriya and M. Uemura. An analysis of the tension field after wrinkling in flat membrane structures. In *IASS Pacific Symposium - Part II On Tension Structures and Space Frames*, Tokyo and Kyoto, 1971.

[5] E. Haug and G.H. Powell. Finite element analysis of nonlinear membrane structures. In *IASS Pacific Symposium - Part II On Tension Structures and Space Frames*, Tokyo and Kyoto, 1971.

[6] A.C. Pipkin. The relaxed energy density for isotropic elastic membranes. *Journal of Applied Mathematics*, 36:85–99, 1986.

[7] D.G. Roddeman. Finite-element analysis of wrinkling membranes. *Comm. Appl. Num. Meth.*, 7:299–307, 1991.

[8] N. Bauer. Zur Darstellung von Falten in Membranen mit Hilfe der Methode der Finiten Elemente. Technical report, Mitteilung 33, SFB 64 University of Stuttgart, 1975.

[9] J.G. Teng, S.F. Chen and J.L. Hu. A finite–volume method for deformation analysis of woven fabrics. *Int. J. Num. Meth. Eng.*, 46:2061–2098, 1999.

[10] F. Cirak, M. Ortiz and P. Schröder. C^1–conforming subdivision elements for thin–shell analysis. In *European Congress on Computational Methods in Applied Sciences and Engineering*, Barcelona, 2000. ECCOMAS.

[11] F. Cirak, M Ortiz and P. Schröder. Subdivision surfaces: A new paradigm for thin–shell finite–element analysis. *Int. J. Num. Meth. Eng.*, 47:2039–2072, 2000.

[12] J.C. Simo and T.J.R. Hughes. *Computational Inelasticity*. Springer, 1998.

[13] J.C. Simo, J.G. Kennedy and S. Govindjee. Non-smooth multisurface plasticity and viscoplasticity. loading/unloading conditions and numerical algorithms. *Int. J. Num. Meth. Eng.*, 26:2161–2185, 1988.

[14] P. Contri and B.A. Schrefler. A geometrically nonlinear finite element analysis of wrinkled membrane surfaces by a no–compression model. *Comm. Appl. Num. Meth.*, 4:5–15, 1988.

[15] K. Schweizerhof and E. Ramm. Displacement dependent loads in nonlinear finite element analysis. *Comp. Struct.*, 18(6):1099–1114, 1983.

[16] O.C.Zienkiewicz and R.L. Taylor. *The Finite Element Method*. Butterworth–Heinemann, 2000.